International Journal of Neural Systems, Vol. 17, No. 2 (2007) 79–86

World Scientific
www.worldscientific.com

ROLE OF REFRACTORY PERIOD IN HOMOCLINIC MODELS OF NEURAL SYNCHRONIZATION

A. MONTINA
Dipartimento di fisica, Università di Firenze, via Sansone 1, 50019 Sesto Fiorentino (FI), Italy
almont@inoa.it

C. MENDOZA
Institute of Physics, Pontifical Catholic University of Valparaíso, 234-0025 Valparaíso, Chile
and
Istituto Nazionale di Ottica Applicata, Largo E. Fermi 6, 50125 Firenze, Italy
cmendoza@ucv.cl

F. T. ARECCHI
Dipartimento di fisica, Università di Firenze, via Sansone 1, 50019 Sesto Fiorentino (FI), Italy
and
Istituto Nazionale di Ottica Applicata, Largo E. Fermi 6, 50125 Firenze, Italy
tito.arecchi@inoa.it

We study the properties of a homoclinic model of neuron by introducing a suitable one-dimensional map. We show that the system is characterized by a response time to external signals which is a decreasing function of the signal strength, in contrast to excitable models whose response time is signal-independent. In a one-dimensional array of these systems with bidirectional coupling, we observe a sudden transition to a synchronized state at a certain value of the coupling strength. The transition occurs when the response time of a site to the signals of the adjacent sites is of the order of refractory time. Near the transition, we find an intermittent behavior due to the competition between a turbulent and a synchronized state. The observed behavior distinguishes homoclinic systems from excitable systems.

1. Introduction

Homoclinic Chaos (HC)[1] is the name given to the chaotic behavior of a dynamical system characterized by the homoclinic return of the phase space point to a saddle focus (SF) where the local contraction and expansion rates fulfill the Shilnikov condition;[2] thus the local condition on SF determines the global behavior. HC is characterized by identical spikes occurring with non identical interspike intervals (ISI); thus the statistics of ISI provides an efficient time code for processing information.[3] Applications of HC to cognitive tasks performed by large assemblies of neurons have been hypothesized,[3] even though no direct evidence is yet available. In this regard, a hint is provided at the spatial level by the crucial role of synchronization of different neurons in feature binding;[4,5] this means that a large assembly of neurons in a cortical module convenes toward a specific perception, provided that the majority of neurons have spiking action potentials which are correlated by synchronization. For this purpose HC is a very attractive system, since

it is easily synchronized either by a weak external perturbation[1] or by mutual coupling among identical HC systems;[6,7] such a *propensity* to synchronization is highest in HC as compared to other chaotic systems.[8]

The Shilnikov condition refers to three coupled equations, thus it requires a three dimensional (3D) phase space and indeed a laboratory evidence of it was provided by a laser set-up which was initially modeled by three coupled equations.[9] However, to provide an accurate fitting of model expectations with experimental data over a long time, it was necessary to recur to a 6 equation model.[10] Most biochemical clocks are adaptive clocks which can adjust their period in presence of an appropriate stimulus;[11] but in general they are ruled by a large number of equations, as known in the Hodgkin-Huxley model[12] or in the models for Belousov-Zhabotinsky chemical oscillations.[13]

What is common to all models displaying HC is that out of $N > 3$ variables only 3 are relevant at the SF, since the other $N - 3$ are much faster at SF and hence they can be *adiabatically eliminated.*[14] This means that for $(N - 3)$ variables we can take the local equilibrium solutions and replace the corresponding values in the remaining 3 equations which provide the Shilnikov behavior at SF.

The homoclinic return to SF may not be sufficient to assure a regular motion far away from SF. In the laser experiment, a second stabilizing fixed point is represented by a saddle node (SN) where the laser intensity goes to zero.[8,10] This way, the phase space orbit is made of the heteroclinic connection between SF and SN and chaos is confined to a small region around SF. The SN provides a fixed refractory time at each *ISI*, where the system is practically insensitive to external perturbations.

From now on, we extend the term HC to the heteroclinic connection from SF (obeying Shilnikov condition) to SN and vice versa. The relevant features common to any HC, independently of the number $N \geq 3$ of equations, are for each *ISI*:

i. a long but erratic permanence in a small neighborhood of SF, that we call *laminar region*;
ii. short spike of fixed duration, corresponding to the heteroclinic connection between the two fixed points;
iii. fixed *refractory time* T_r at SN; it may be a sizable fraction of *ISI*
iv. as for the *sensitivity* to an external perturbation, it is very high near SF, and very low elsewhere[15]

Thus, for all purposes, the dynamical signal can be seen as a sequence of stereotyped short spikes with fixed duration and relatively small amplitude fluctuations, separated by blank intervals of variable duration (*ISI*), a fraction of which (refractory time) is always the same. Neurons can display a similar behavior, they can generate spikes with erratic *ISI* and have a fixed refractory time after each spike generation, where the neurons are insensitive to external signals.

In this article, we introduce a one-dimensional return map, described by a variable x, in order to capture these characteristics with small numerical efforts. We show that the refractory time is an important ingredient for synchronization of coupled HC systems. If an external one-step signal is provided when the system is near the SF, a finite time T_g is necessary to generate a spike. T_g decreases by increasing the intensity of the external signal. This behavior is quite different from that of an excitable system. Excitability is indeed a threshold phenomenon, but once the threshold is overcome, the response time is nearly independent of the signal amplitude. We show that, for a one-dimensional array with bidirectional couplings, the intersite correlation has a sudden increase above a threshold value ϵ_{thr} of the coupling parameter, due to synchronization of the array. The transition value is reached when the generation time T_g becomes of the order of the refractory time T_r. Near ϵ_{thr} we observe an intermittent behavior of the array, due to competition between the synchronized state and a turbulent state. We characterize the transition by means of the statistical one-site behavior and the two-site correlation.

2. HC Dynamics in Terms of One-Dimensional Maps

The evolution of a HC system can be studied over discrete time steps by means of a one-dimensional return map. We indicate the one-dimensional variable at time t as $x(t)$. We consider a map with a fixed point at $x = 0$ and a very slow dynamical evolution around it. When $x(t) > 1$, at next step the variable

jumps to a region around 0. An additional variable y is introduced which is 1 when a jump occurs and 0 elsewhere. It gives spikes with constant amplitude and one-time step duration. The map evolution is defined as follows

$$x(t+1) = a_0 + a_1 x(t) + a_2 x(t)^2 + a_3 x(t)^3 \quad \text{if } x(t) \leq 1 \quad (1)$$

$$x(t+1) = b \cdot [x(t) - 1] + c \quad \text{if } x(t) > 1 \quad (2)$$

b is a squeezing factor which re-injected the dynamical point close to the origin, whenever x becomes greater than 1. In order to account for the refractory region, we introduce another ingredient. When a spike is generated, the variable x is frozen for T_r steps, then it restarts the cycle.

For $a_0 = 0$, $x = 0$ is a stationary state and it is unstable for $a_1 > 1$. If a_1 is slightly larger than 1, the variable stays near 0 for a large fraction of the *ISI*. With this choice of a_1, x grows only if it is positive. Thus, we have to set $c \geq 0$ in order to have a monotonic increase of the variable in the laminar region. We take $b \ll 1$ and $c = 0$, this means that when x becomes greater than 1, the variable jumps very close to the stationary state. The cubic map (linear and cubic terms) would be sufficient to describe the relevant dynamical features of single systems. However, when we consider an array of coupled systems, we should let also negative x values, thus, x has to increase also in a region below $x = 0$. This is possible if a quadratic term is present, with $a_0 > 0$ and $a_1 = 1$. In this case, $x = 0$ is not a fixed point, however with $a_0 \ll 1$, we still have a laminar region with slow dynamics near 0. Such map setting will be considered in Sec. 7.

In Fig. 1, we report $x(t)$ and $y(t)$ for $T_r = 50$, $a_0 = 0$, $a_1 = 1.01$, $a_2 = 0.943$, $a_3 = 0.66$ and

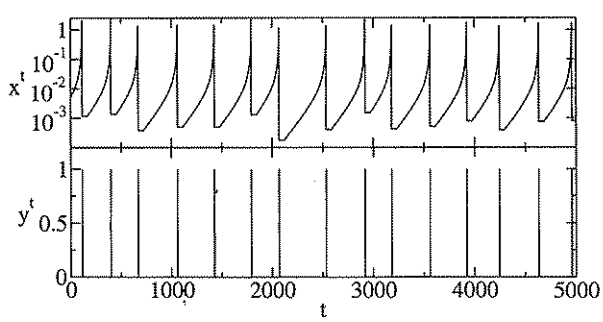

Fig. 1. $x(t)$ and $y(t)$ for $T_r = 50$, $a_0 = 0$, $a_1 = 1.01$, $a_2 = 0.943$ and $a_3 = 0.66$.

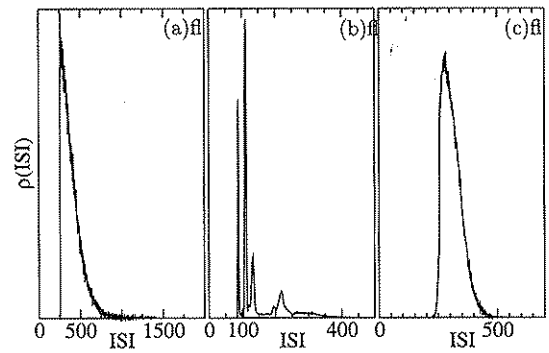

Fig. 2. *ISI* distribution of one map (a) and an array of 50 maps with bidirectional coupling for $\epsilon = 1.5 \times 10^{-2}$ (b) and $\epsilon = 2 \times 10^{-2}$ (c).

$b = 10^{-3}$. For these values the spikes occur with non identical time separation. The corresponding *ISI* distribution is reported in Fig. 2(a).

3. One-Dimensional Array of Maps with Bidirectional Coupling

In the following, we consider a one-dimensional array of maps with bidirectional coupling. We indicate the array sites with a suffix. Equation (1) becomes

$$x_n(t+1) = a_0 + a_1 x_n(t) + a_2 x_n(t)^2 + a_3 x_n(t)^3 + \epsilon[y_{n+1}(t) + y_{n-1}(t) - 2y_n(t)] \quad \text{if } x_n \leq 1 \quad (3)$$

We realize the coupling by means of the stereotyped variables $y_n(t)$.

Since the refractory time starts when a spike is generated, the coupling term $-2\epsilon y_n(t)$ of Eq. (3) is unimportant for the dynamics and the maps undergo only a positive perturbation given by $\epsilon[y_{n+1}(t) + y_{n-1}(t)]$. If site n generates a spike, the coupling between n and $n+1$ gives a positive signal to site $n+1$, whose effect is the removal of x_{n+1} from the region near the fixed point 0. After a time T_g, site $n+1$ generates a new spike. T_g takes the maximum value T_g^M if site n generates the spike when $x_{n+1} = 0$. It is clear that T_g^M decreases by increasing ϵ. We report in Fig. 3 the maximum generation time T_g^M as a function of the amplitude of the external signal A_s, for two sets of the parameters. T_g^M is independent of the refractory time T_r and b.

In an array with bidirectional coupling, it is possible to identify two dynamical regimes. Suppose that site n generates a spike when site $n+1$ is in the

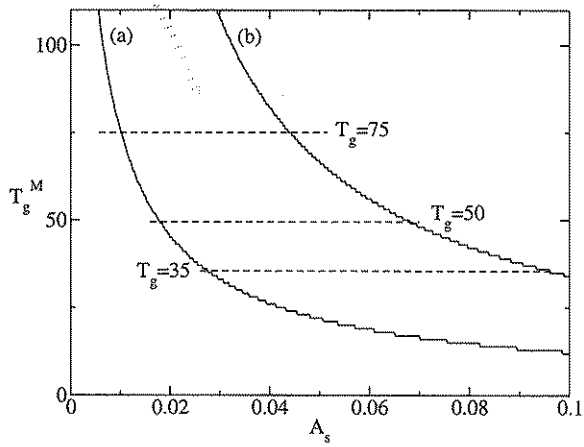

Fig. 3. Maximum generation time T_g^M as a function of the amplitude of the one-step signal for (a) $a_1 = 1.01$, $a_2 = 0.943$, $a_3 = 0.66$ and (b) $a_1 = 1.001$, $a_2 = 0.3$, $a_3 = 0$.

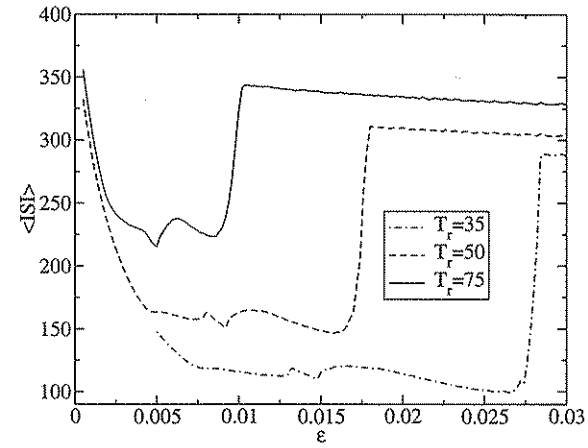

Fig. 4. Mean *ISI* at one site as a function of the coupling parameter ϵ, for $a_1 = 1.01$, $a_2 = 0.943$, $a_3 = 0.66$ and $b = 10^{-3}$ and number of sites $N_s = 50$.

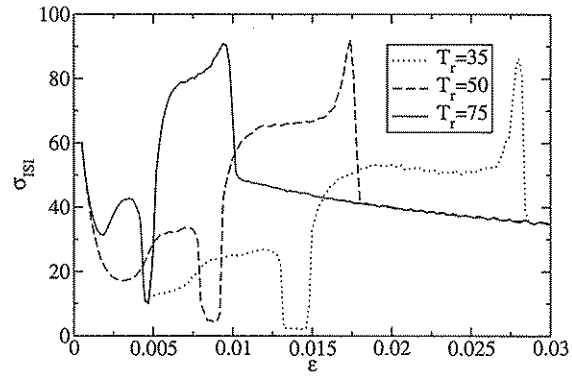

Fig. 5. Standard deviation of the *ISI* distribution at one site as a function of the coupling parameter ϵ. The parameters are the same as in Fig. 4.

laminar region. Because of the coupling, site $n+1$ generates a spike at a time less or equal to $T_g^M(\epsilon)$. If $T_g^M(\epsilon) < T_r$, site n receives a new spike from site $n+1$ when it is in the refractory region. Thus, the bidirectional coupling acts as a unidirectional one. Conversely, if $T_g^M(\epsilon) > T_r$ a back-action of the $n+1$ site on the n site is possible. The transition between these two different regimes gives a sudden change in the behavior of the array. The threshold value ϵ_{thr} of the transition is given by the equation $T_g^M(\epsilon_{thr}) = T_r$. In Fig. 2b–c, the *ISI* distributions of 50 sites are plotted for $\epsilon = 1.5 \times 10^{-2}$ and 2×10^{-2}. The refractory time is 50 and the other parameters are as in Fig. 1. We have taken open boundary conditions. In the first case, ϵ is below the threshold value and $T_g^M(\epsilon) = 56$, which is greater than T_r. Two narrow peaks are present at $ISI \simeq 88$ and 111. This last value is twice T_g^M and corresponds to the following event: the site n generates a spike when one of the two adjacent sites, say $n-1$, is in the refractory period and the other one is near the fixed point. Site $n+1$ generates a new spike after the time T_g and induces the site n to produce another spike after $2T_g^M$. The first peak has a similar explanation, but in this case both adjacent sites are near the fixed point and generate a spike after T_g^M. The second spike of site n is induced by a doubled signal with amplitude 2ϵ and generation time $T_g^M(2\epsilon) = 32$, which, summed to $T_g^M(\epsilon)$, gives the mean $ISI = 88$ of the first peak. The greater *ISI* values are given when both the adjacent sites are in the refractory period during the spiking of site n. In Fig. 2c, the coupling parameter is above ϵ_{thr} and $T_g^M(\epsilon) > T_r$, thus the previous feedback mechanisms are inhibited and the peak structure disappears.

In Figs. 4 and 5, the mean and standard deviation of the *ISI* distribution are respectively plotted as functions of the coupling parameter ϵ, for three values of the refractory time, for a number of sites $N_s = 50$. The curves do not considerably change by increasing the array size. In fact, from $N_s = 15$ to above we do not observe sizable changes in Figs. 4 and 5. Increasing ϵ, the mean *ISI* rapidly reduces until it reaches a nearly constant value. Slightly below the threshold value ϵ_{thr}, given by $T_g^M(\epsilon_{thr}) = T_r$, the mean *ISI* suddenly increases with a maximum obtained at the threshold value. Above

ϵ_{thr}, the slope changes and becomes negative. A similar sudden slope change is observed for the standard deviation σ_{ISI}. Slightly below ϵ_{thr}, σ_{ISI} increases, it reaches a maximum and again decreases, until it suddenly changes slope at ϵ_{thr}. Note that above the threshold, the value of σ_{ISI} is practically independent of the refractory time and lies on a universal curve.

The one site statistics says nothing about map synchronization. For this reason, we have studied the intersite correlations, evaluating the probability distribution of the time difference between spikes of adjacent sites. When the coupling is zero, this distribution is flat, i.e., the information on a site gives no information on the other ones. Increasing the coupling, we observe the birth of peaks near the zero value of the time difference, due to the time correlation between the spikes of adjacent sites. We evaluated the distribution on a time rate of several mean *ISI* and calculated the corresponding entropy as a function of ϵ for different values of the parameters. Also in this case, we find that the slope suddenly decreases above the ϵ_{thr}, i.e., the intersite correlations rapidly increases, indicating the beginning of synchronization between the maps. In Fig. 6, the entropy of the time difference distribution is reported for some values of the parameters. Note that the entropy is defined besides a constant, which depends on the histogram interval used to construct the probability distribution. For convenience, in figure we have vertically translated the curve

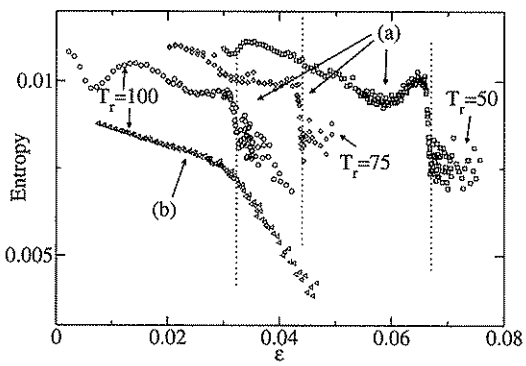

Fig. 6. Entropy of the intersite time difference distribution as a function of ϵ, for $a_1 = 1.001$, $a_2 = 0.3$, $a_3 = 0$. b is 0.03 (a) and 0.1 (b). For (a) the three values 50, 75 and 100 of the refractory time are considered. For (b) T_r is equal to 100. The vertical lines correspond to the values of ϵ for which the refractory time T_r is equal to the generation time $T_g^M(\epsilon)$.

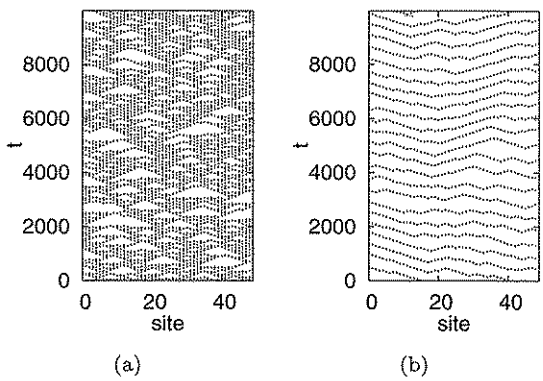

Fig. 7. Space-time position of the spikes for $a_1 = 1.001$, $a_2 = 0.3$, $a_3 = 0$, $b = 0.03$ and (a) $\epsilon = 6 \cdot 10^{-2}$, (b) $\epsilon = 7 \cdot 10^{-2}$.

(b) with respect the other ones in order to not overlap them. In Fig. 7 we report the space-time position of the spikes for two values of ϵ. Below the threshold value of ϵ (a) we observe an intermittent behavior, where regions without activity are suddenly created and swallowed up by high activity regions. Above the threshold (b) the sites are completely synchronized. By "synchronized" we do not mean "isochronous", in which case the space-time plot would be a collection of strictly horizontal lines, but that adjacent sites have spikes very close by in time (separation smaller than T_r). As a consequence, we observe large time fluctuations between sites far away from each other. Strict isochronism implying long range synchronization would emerge if we consider long range, rather than nearest neighbor coupling. The intermittent dynamics can easily be explained. When ϵ is near ϵ_{thr}, the generation time T_g has a maximum slightly above the refractory time T_r, thus there is a large probability to have a T_g less than T_r. When this simultaneously occurs in a small region, there the system remains locally to a quasi-stationary state with $x_n \simeq 0$. The neighboring sites with high spiking rate move the stationary sites away from the fixed unstable point. This perturbation propagates inside the quiescent region with a velocity of the order of $1/\langle T_g \rangle$, creating the triangular structures of Fig. 7(a). Above ϵ_{thr}, T_g becomes smaller than T_r in all the array and the high spiking regions disappears completely (Fig. 7b).

4. Delayed Refractory Time

In the previous sections, we have considered a refractory period which begins as soon as a spike

is generated. This implies that the coupling is ineffective on site n when $y_n = 1$, thus the term $\epsilon(y_{n+1} + y_{n-1} - 2y_n)$ can be replaced by $\epsilon(y_{n+1} + y_{n-1})$ without affecting the dynamics. These considerations do not apply if we delay the onset of the refractory period by one step. In this case, when x_n jumps from a value greater than 1 to a value near 0, at the next time step, when $y_n = 1$, the variable evolution is given by Eq. (1) and the system is still sensitive to the coupling. Thus, the previous replacement of the coupling term is not possible. Here, some care is necessary for the choice of the parameters a_k. We have previously put $a_0 = 0$ and a_1 slightly greater than 1, which corresponds to $x_n = 0$ being an unstable point. Because of the negative term $-2\epsilon y_n$, the variable x_n can take a negative value and evolve to a stable negative fixed point. In order to have a growth of x_n also for slightly negative values, we put $a_1 = 1$ and a_0 positive. The slow dynamics near $x_n = 0$ is maintained if $a_0 \ll 1$.

The term $-2\epsilon y_n$ is different from zero and equal to -2ϵ when the map returns to the laminar region. Thus, the introduced delay is practically equivalent to a zero delay with $c = -2\epsilon$ in Eq. (2).

Also in this different situation, there is a threshold value ϵ_{thr} for the coupling above which the sites synchronize. The transition occurs again when T_g^M is of the order of T_r, indicating the essential role of the refractory period. As a difference with respect to the previous case, the synchronized system is not chaotic but periodic. Furthermore, we observe near the threshold an intermittent jump between a completely synchronized spiking regime and an unsynchronized turbulent dynamics with larger spiking rate.

In Fig. 8, the mean *ISI* and the standard deviation are reported as a function of the coupling parameter, for $a_0 = 1.e-5$, $a_1 = 1$, $a_2 = 0.943$, $a_3 = 0.66$, $b = 10^{-2}$ and $N_s = 200$. The quantities were evaluated after a transient of 2×10^6 time steps and over 2×10^6 time steps.

The vertical lines correspond to the values of ϵ for which the refractory time T_r is equal to the generation time $T_g^M(\epsilon)$, which has been evaluated applying to a single map a one time step pulse of amplitude ϵ, when $x_n = 0$. Note that, in the region of the transition, there are large statistical fluctuations of *ISI* and standard deviation. This is due to the large time scale of the intermittent jumps between the periodic regime and the aperiodic one.

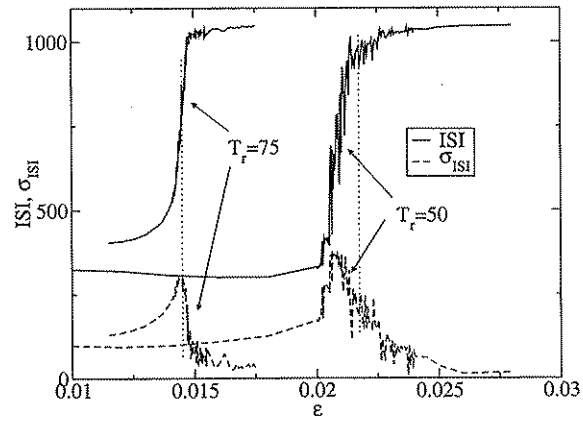

Fig. 8. Mean *ISI* and standard deviation as a function of ϵ with $a_0 = 10^{-5}$, $a_1 = 1$, $a_2 = 0.943$, $a_3 = 0.66$, $b = 10^{-2}$ and $N_s = 200$. The refractory time is del ayed by a one time step.

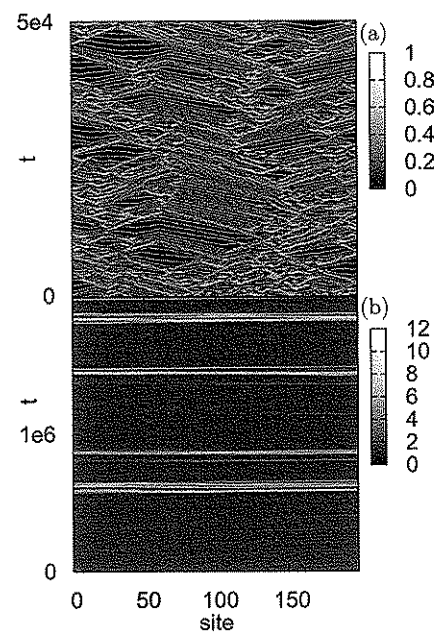

Fig. 9. Space-time distribution of spikes with parameters of Fig. 8 and $\epsilon = 2 \times 10^{-2}$ (a), $\epsilon = 2.1 \times 10^{-2}$ (b). The grayscale represents the number of spikes in a time interval of 100 (a) and 1000 (b) steps.

In Fig. 9, the space-time distribution of spikes is reported for $\epsilon = 2 \times 10^{-2}$ (a) and $\epsilon = 2.1 \times 10^{-2}$ (b). We have smoothed the distribution integrating over temporal intervals of 100 (a) and 1000 (b) steps. In the first case, there are several clusters of synchronized sites with different *ISI* and regions with high spiking rates. This complex structure is created by

the competition between the synchronized and turbulent states. The coupling parameter is below the threshold and the maximum generation time T_g^M is slightly larger than the refractory time T_r. In the second case, T_g^M is smaller and the synchronization of sites becomes possible. The corresponding mean *ISI* is about 1000. On large time scales, intermittent jumps between this synchronized state and a turbulent state (bright regions) with a mean *ISI* of about 300 occur. This behavior is similar to that found in neuronal in-vitro networks, where events with high activity are generated on large time scales with respect to the mean *ISI*.

We have shown that, if the generation time is larger than the refractory time, when map n produces a spike at the time T, it leads an adjacent site to create another spike at a time $T + T_g$, which acts again on map n because of the bidirectional coupling. This feedback leads to a turbulent behavior. The feedback is inhibited when $T_g < T_r$, i.e., with sufficiently large coupling parameters. With more complex networks, for example with small world coupling, this feedback mechanism can still be present for smaller T_r or larger ϵ, since the feedback signal is transmitted through several maps, before returning to the originating site. If the number of passes of the feedback line is n_f, the turbulent state is inhibited when $n_f T_g < T_r$. Each site can have several feedback lines and n_f can depend on the site and the line. In this case very complex space-time structures could be possible.

5. Conclusion

In this work, we have considered a homoclinic system as a model of neuron. This system is characterized by particular features. It has a long and erratic permanence very close to a saddle focus and, when it escapes far away from this fixed point, generates a short spike output. After the spiking, it goes into a refractory period, during which it is frozen and insensitive to the external signals. As a consequence of these features, the homoclinic system is able to respond also to weak signals and its response time, or generation time, is a decreasing function of the amplitude signal. In contrast, other models of neurons respond only if the signal amplitude is greater than a threshold value and their response time is independent from the amplitude of the perturbation and almost instantaneous. In this paper, the homoclinic system has been implemented by a one-dimensional return map. We then studied a one-dimensional array of homoclinic systems with bidirectional coupling and have shown that a sudden synchronization occurs when a threshold value of the coupling strength is reached. The observed transition is due to the dependence of the generation time T_g on the coupling parameter and it occurs when T_g becomes of the order of the refractory time. The transition associated with this competition between the T_g and the refractory time is hardly observable in excitable systems, which are typically characterized by two very different time scales, with the generation time much smaller than the refractory time and nearly independent of the coupling strength.[16]

Our study introduces a new feature in the neural dynamical behavior and it is interesting to investigate if other models can have a coupling-dependent response time for some values of their parameters.

Acknowledgement

Work supported by contract "Ente Cassa di Risparmio di Firenze 2004" n. 2004.0229, "dinamiche cerebrali caotiche".

References

1. E. Allaria, F. T. Arecchi, A. Di Garbo and R. Meucci, *Phys. Rev. Lett.* **86** (2001) 791.
2. L. P. Sil'nikov, *Sov. Math. Dokl.* **6** (1965) 163.
3. F. T. Arecchi, *Physica A* **338** (2004) 218, and references therein.
4. C. Von der Malsburg, *The Correlation Theory of Brain Function*, reprinted in E. Domani, J. L. Van Hermmen and K. Schulten (eds.), *Models of Neural Networks II*, Springer, Berlin (1981).
5. W. Singer and E. C. M. Gray, *Annu. Rev. Neurosci.* **18** (1995) 555.
6. I. Leyva, E. Allaria, S. Boccaletti and F. T. Arecchi, *Chaos* **14** (2004) 118.
7. I. Leyva, E. Allaria and S. Boccaletti and F. T. Arecchi, *Phys. Rev. E.* **68** (2003) 066209.
8. F. T. Arecchi, E. Allaria and I. Leyva, *Phys. Rev. Lett.* **91** (2003) 234101.
9. F. T. Arecchi, W. Gadomski, A. Lapucci, H. Mancini, R. Meucci and J. A. Roversi, *J. Opt. Soc. Am. B* **5** (1988) 1153.
10. A. N. Pisarchik, R. Meucci and F. T. Arecchi, *Eur. Phys. J. D* **13** 385–391.
11. F. T. Arecchi, *Recent Advances in Metrology and Fundamental Constants* (Int. School of Physics

E. Fermi, course CXLVI, (eds.) T. J. Quinn, S. Leschiutta and P. Tavella, Varenna 2000), IOS Press Amsterdam (2001) 781.
12. A. L. Hodgkin and A. F. Huxley, *Journal of Physiology* **117** (1952) 500.
13. F. Argoul, J. Huth, P. Merzeau, A. Arnéodo and H. L. Swinney, *Physica D* **62** (1993) 170.
14. H. Haken, *Synergetics* Springer, Berlin (1983).
15. I. Tokuda, J. Kurths, E. Allaria, R. Meucci, S. Boccaletti and F. T. Arecchi, *Predicting Phase Synchronization for Homoclinic Chaos in a CO2 Laser* ECC8: Proc AIP Conf. **742**, AIP-Melville New York (2004) 345.
16. J. Keener and J. Sneed, *Mathematical Physiology* (Springer-Verlag, New York, 1998).